CROATIAN - USA WORKSHOP
on
MESOMETEOROLOGY

Ekopark Kraš Resort near Zagreb, Croatia

18-20 June 2012

ORGANIZING INSTITUTIONS

Meteorological and Hydrological Service of Croatia
School of Meteorology, University of Oklahoma
Geophysical Institute, University of Zagreb

ABSTRACTS OF INVITED LECTURES

Theory of slope flows and low-level jets

Alan Shapiro*

**School of Meteorology, University of Oklahoma, Norman, Oklahoma, USA*

1. Introduction

In this presentation we will examine theories for two classes of mesoscale atmospheric phenomena associated with sloping terrain: slope flows (katabatic and anabatic winds) and the nocturnal low-level jet. The theories we consider are fairly idealized and designed to provide a conceptually simple account of some of the main dynamical features of these flows.

Slope winds are thermally driven motions found in regions of complex terrain at all latitudes (Whiteman 1990, Egger 1990). When a sloping surface is heated or cooled, a temperature difference is set up between the air in the surface layer and the environmental air at the same altitude. The buoyancy field associated with this temperature difference projects in the along-slope direction and induces an along-slope flow. In areas where basins are largely sheltered from synoptic effects, slope flows are the building blocks of local weather. Even in cases where synoptic forcing is important, pronounced slope flow signals may still be apparent. In regions where heavily industrialized population centers extend across variable topography, these local winds exert major controls over energy usage, visibility, fog formation, and air pollutant dispersion (Lu and Turco 1994, Fernando et al. 2001, Hunt et al. 2003, Brazel et al. 2005). In agricultural regions, these winds significantly affect microclimates. They also need to be taken into account in aerial spraying and firefighting operations. On the larger scale, persistent katabatic winds cover vast areas of the earth (e.g., Greenland, Antarctica), and play an important role in the weather and climate of those areas (Parish and Waight 1987, Gallee and Schayes 1994, Renfrew 2004).

Katabatic and anabatic winds can be described in their most basic forms as turbulent natural convection flows along cooled/heated sloping surfaces in a stratified environment. Katabatic flows in particular are quite shallow (typical jet maximum occurs in the height range between 1 to 100 m above ground level), and are therefore poorly resolved in most numerical models. Although much progress has been made in the conceptual understanding and quantitative description of slope winds, long-standing difficulties with modeling stably-stratified turbulent flows along slopes, and the variety of flow interactions caused by complex topography and surface inhomogeneity (e.g. from irregular snow cover, cloud cover, or topographic shading) make the dynamics of these flows a rich and challenging area of study.

The nocturnal low-level jet (LLJ) is an atmospheric boundary-layer phenomenon most extensively documented over the Great Plains of the United States (e.g., Blackadar 1957, Hoecker 1963, Bonner 1968, Mitchell et al. 1995, Stensrud 1996, Zhong et al. 1996, Whiteman et al. 1997, Banta et al. 2002, Song et al. 2005, Banta 2008) but also observed at many other locations worldwide (Sladkovic and Kanter 1977, Stensrud 1996, Beyrich et al. 1997, and Baas et al. 2009). The jet typically begins to develop around sunset, under dry cloud-free conditions conducive to strong radiative cooling, reaches its peak intensity in the early morning hours, and then decays after dawn, with the onset of daytime convective mixing. It is characterized by an anticyclonic turning of the wind vector with time. The wind maximum typically occurs at levels less than 1 km above ground level, but frequently occurs at levels less than 500 m above ground level. The peak jet winds are often supergeostrophic by ~70%, but can exceed the geostrophic values by several hundred per cent in strong cases (e.g., Hoecker 1963, Bonner 1968, Brook 1985). Vertical profiles of LLJ winds have distinctive and graceful shapes characterized by

large curvature in the vicinity of a pronounced wind maximum (Fig. 1). Over the Great Plains, the nocturnal low-level jet is sometimes also known as the Southerly Jet because of its climatological association with strong southerly geostrophic winds.

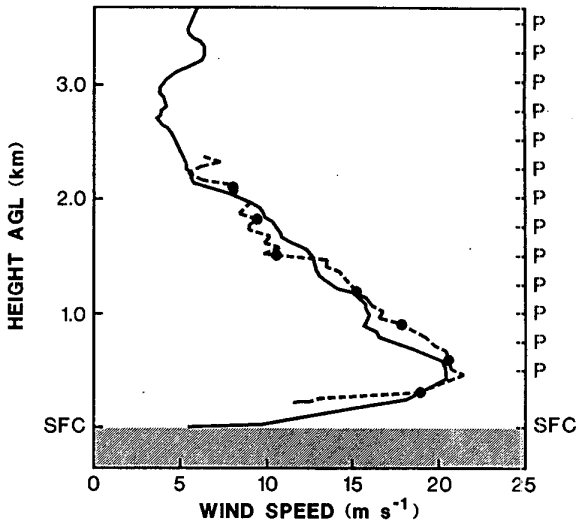

Figure 1. Winds in a nocturnal low-level jet (from Stensrud *et al*. 1990) from a Velocity Azimuth Display (VAD) analysis using WSR-88D data (dashed line) and from the Cross-chain Loran Atmospheric Sounding System (CLASS).

2. Governing equations (general formulation)

To make the analyses of slope flows and LLJs tractable, while allowing the main features of these flows to emerge, we restrict attention to planar slopes (constant slope angle α), a constant environmental potential temperature gradient γ, constant Coriolis parameter f, and constant eddy viscosity ν and thermal diffusivity κ coefficients. We work in a slope-following coordinate system with the x axis directed down the slope, the y axis directed across the slope along constant topographic height lines, and the z axis directed normal to the slope. The components of the velocity vector $\mathbf{v}$ in these three directions are u, v, and w, respectively. In this slope-following coordinate system, the Boussinesq equations of motion, thermal energy and mass conservation (incompressibility condition) are

$$\frac{\partial u}{\partial t} + \mathbf{v}\cdot\nabla u = -\frac{1}{\rho_r}\frac{\partial p'}{\partial x} + fv - g\frac{\theta'}{\theta_r}\sin\alpha + \nu\nabla^2 u, \tag{1}$$

$$\frac{\partial v}{\partial t} + \mathbf{v}\cdot\nabla v = -\frac{1}{\rho_r}\frac{\partial p'}{\partial y} - fu + \nu\nabla^2 v, \tag{2}$$

$$\frac{\partial w}{\partial t} + \mathbf{v}\cdot\nabla w = -\frac{1}{\rho_r}\frac{\partial p'}{\partial z} + g\frac{\theta'}{\theta_r}\cos\alpha + \nu\nabla^2 w, \tag{3}$$

$$\frac{\partial \theta'}{\partial t} + \mathbf{v}\cdot\nabla\theta' = \gamma\left(u\sin\alpha - w\cos\alpha\right) + \kappa\nabla^2\theta', \tag{4}$$

$$\nabla\cdot\mathbf{v} = 0, \tag{5}$$

where primes denote perturbation variables, a subscript r denotes a constant reference value, and other symbols have their conventional meanings.

3. Theoretical analyses of slope flows and low-level jets

The presentation will focus on several theoretical models of slope flows and low-level jets. An early milestone in the theory of slope flows was the Prandtl (1942) model for steady, viscous, one-dimensional (1D, flow variables are functions of z only) flow of a non-rotating ($f = 0$) fluid along a

uniformly heated slope. No provision was made for synoptic-scale effects (e.g., an imposed pressure gradient force or external wind). Under the 1D restriction, (5) reduces to $\partial w/\partial z = 0$ which, together with the impermeability condition ($w = 0$ on the slope) shows that $w = 0$ everywhere, and (3) reduces to the quasi-hydrostatic equation ("quasi" since z is a slope-normal coordinate, not a true vertical coordinate). The latter equation together with the 1D restriction on θ' shows that $\partial p'/\partial x = \partial p'/\partial y = 0$ everywhere. Equation (2) together with the no-slip condition and the condition that there be no externally imposed wind then show that $v = 0$ everywhere. Equations (1) and (4) then show that the downslope component of the buoyancy $-g\theta' \sin\alpha / \theta_r$ balances the divergence of the momentum flux $\nu \partial^2 u/\partial z^2$, while the downslope-advection of environmental potential temperature $\gamma u \sin\alpha$ balances the divergence of the heat flux $\kappa \partial^2 \theta'/\partial z^2$. These equations are readily solved analytically. The solution is shown in Fig. 2.

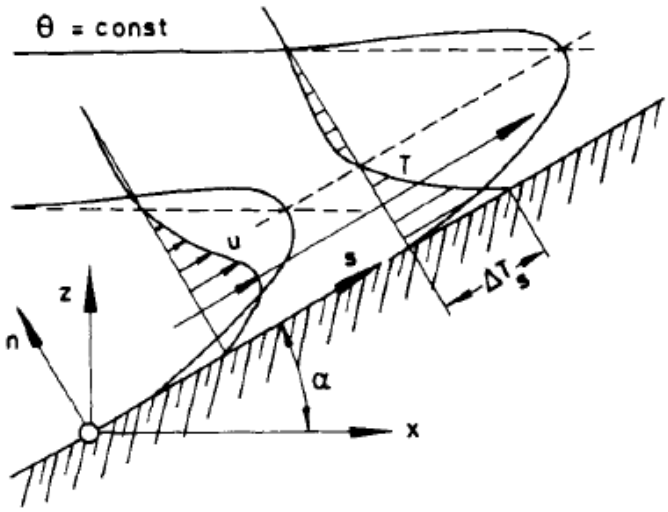

Figure 2. Prandtl solution for velocity and perturbation potential temperature in the boundary layer above a heated slope (from Schumann 1990).

The classical 1D Prandtl model of slope winds has undergone several extensions and refinements, including provision for the Coriolis force (Gutman and Malbakhov 1964, Lykosov and Gutman 1972, Egger 1985, Stiperski et al. 2007, Shapiro and Fedorovich 2008), time dependence, and z-varying ν and κ coefficients (Grisogono and Oerlemans 2001, 2002). Several studies have also examined the role of surface thermal inhomogeneities, considered either as a gradually varying surface buoyancy/buoyancy flux (Shapiro and Fedorovich 2007) or a sharply varying surface buoyancy/buoyancy flux (Egger 1981, Kondo 1984, Shapiro and Fedorovich 2008, Burkholder et al. 2009, Shapiro et al. 2012). A common feature of the inhomogeneously-forced flows was the formation of horizontal intrusions or jets that entered/left the katabatic boundary layer, as shown schematically in Fig. 3.

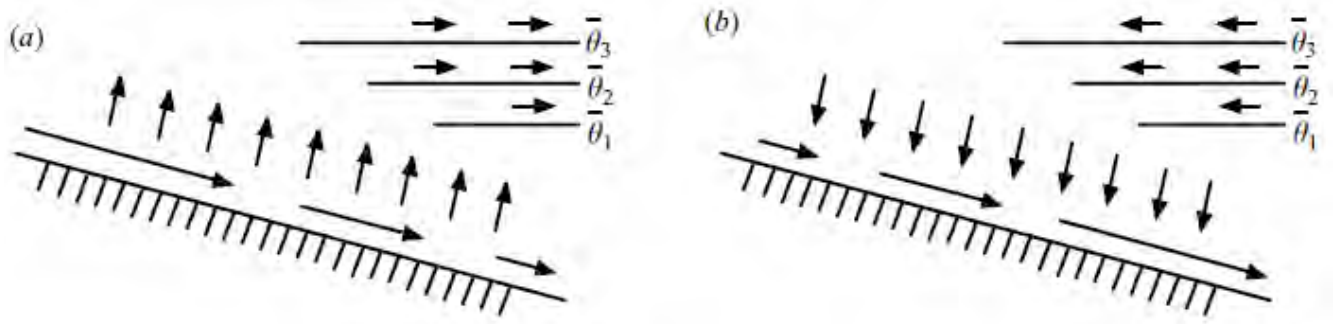

Figure 3. Schematic diagrams of katabatic flows in which the buoyancy (a) increases down the slope, and (b) decreases down the slope (from Shapiro and Fedorovich 2007).

An early milestone in the theory of nocturnal low-level jets was Blackadar's (1957) conceptual view that the jets arise as inertial oscillations that develop in the boundary layer in response to the rapid stabilization of the boundary layer near sunset. During the day, the flow is considered to be in an equilibrium state, with the horizontal pressure gradient force, Coriolis force and frictional force (turbulent stress) balancing each other. When the atmosphere stabilizes, air parcels are suddenly freed of the frictional constraint and accelerate under the resulting force imbalance. The inviscid solution is represented on a hodograph diagram as a circle. The Blackadar inviscid solution was extended by Shapiro and Fedorovich (2010) to include a time-dependent (step-change) eddy viscosity coefficient, thus allowing an evening transition and the no-slip condition to be incorporated directly into the solution. However, neither the Blackadar model nor simple extensions of it can explain (i) the geographical preference of the Great Plains low-level jet (high frequency over the sloping terrain around 100^{o} W), (ii) the physical mechanism for how a jet-like velocity profile can evolve from a well-mixed (uniform) daytime profile, or (iii) how peak jet winds can sometimes exceed geostrophic winds by several hundreds of per cent. We will examine how terrain-associated baroclinicity and the thermal structure of a sloping boundary layer (Holton 1967, Bonner and Paegle 1970, Shapiro and Fedorovich 2009) can shed light on these aspects of LLJs.

References

Banta, R. M, R. K. Newsom, J. K. Lundquist, Y. L. Pichugina, R. L. Coulter, and L. Mahrt, 2002: Nocturnal low-level jet characteristics over Kansas during CASES-99. *Boundary-Layer Meteorol*., **105**, 221-252.

Banta, R. M., 2008: Stable-boundary-layer regimes from the perspective of the low-level jet. *Acta Geophys*., **56**, 58-87.

Beyrich, F, D. Kalass, and U. Weisensee, 1997: Influence of the nocturnal low-level jet on the vertical and mesoscale structure of the stable boundary layer as revealed from Doppler-sodar observations. *Acoustic Remote Sensing Applications*, S. P. Singal, Ed., Narosa Publishing House, 236-246.

Blackadar, A. K., 1957: Boundary layer wind maxima and their significance for the growth of nocturnal inversions. *Bull. Amer. Meteorol. Soc*., **38**, 283-290.

Bonner, W. D., 1968: Climatology of the low level jet. *Mon. Weather Rev*., **96**, 833-850.

Bonner, W. D., and J. Paegle, 1970: Diurnal variations in boundary layer winds over the south-central United States in summer. *Mon. Weather Rev*., **98**, 735-744.

Brazel, A. J., H. J. S. Fernando, J. C. R. Hunt, N. Selover, B. C. Hedquist, and E. Pardyjak, 2005: Evening transition observations in Phoenix, Arizona. *J. Appl. Meteorol*., **44**, 99-112.

Brook, R. R., 1985: The Koorin nocturnal low-level jet. *Bound.-Layer Meteor*., **32**, 133-154.

Burkholder B., A. Shapiro, and E. Fedorovich, 2009: Katabatic flow induced by a cross-slope band of surface cooling. *Acta Geophys*., **57**, 923-949

Egger, J., 1981: On the linear two-dimensional theory of thermally induced slope winds. *Beitr. Phys. Atmosph.*, **54**, 465-481.

Egger, J., 1985: Slope winds and the axisymmetric circulation over Antarctica. *J. Atmos. Sci.*, **42**, 1859-1867.

Egger, J., 1990: Thermally forced flows: theory. *Atmospheric Processes Over Complex Terrain*, W. Blumen, Ed., Amer. Meteor. Soc., 43-58.

Fernando, H. J. S., S. M. Lee, J. Anderson, M. Princevac, E. Pardyjak, and S. Grossman-Clarke, 2001: Urban fluid mechanics: air circulation and contaminant dispersion in cities. *Environ. Fluid Mech.*, **1**, 107-164.

Gallee, H., and G. Schayes, 1994: Development of a 3-dimensional meso-γ primitive equation model: katabatic winds simulation in the area of Terra Nova Bay, Antarctica. *Mon. Weather Rev.*, **122**, 671-685.

Grisogono, B., and J. Oerlemans, 2001: Katabatic flow: Analytic solution for gradually varying eddy diffusivities. *J. Atmos. Sci.*, **58**, 3349-3354.

Grisogono, B., and Oerlemans, 2002: Justifying the WKB approximation in pure katabatic flows. *Tellus A*, **54**, 453-462.

Gutman, L. N., and V. M. Malbakhov, 1964, On the theory of katabatic winds of Antarctic, *Met. issled.*, **9**, (in Russian) 150-155.

Hoecker. W. H., 1963: Three southerly low-level jet systems delineated by the Weather Bureau special pibal network of 1961. *Mon. Weather Rev.*, **91**, 573-582.

Holton, J. R., 1967: The diurnal boundary layer wind oscillation above sloping terrain. *Tellus*, **19**, 199-205.

Hunt, J. C. R., H. J. S. Fernando, and M. Princevac, 2003: Unsteady thermally driven flows on gentle slopes. *J. Atmos. Sci.*, **60**, 2169-2182.

Kondo, H., 1984: The difference of the slope wind between day and night. *J. Meteorol. Soc. Japan*, **62**, 224-233.

Lu, R., and R. P. Turco, 1994: Air pollutant transport in a coastal environment. Part I: Two-dimensional simulations of sea-breeze and mountain effects. *J. Atmos. Sci.*, **51**, 2285-2308.

Lykosov, V. N., and L. N. Gutman, 1972: Turbulent boundary layer above a sloping underlying surface. *Izv. Acad. Sci. USSR, Atmos. Ocean. Phys.*, **8**, 799-809.

Mitchell, M. J., R. W. Arritt, and K. Labas, 1995: A climatology of the warm season Great Plains low level jet using wind profiler observations. *Wea. Forecasting*, **10**, 576-591.

Parish, T. P., and K. T. Waight, 1987: The forcing of antarctic katabatic winds. *Mon. Weather Rev.*, **115**, 2214-2226.

Prandtl, L., 1942: *Führer durch die Strömungslehre*, Vieweg und Sohn, Braunschweig, 382 pp.

Renfrew, I. A., 2004: The dynamics of idealized katabatic flow over a moderate slope and ice shelf. *Q. J. Roy. Meteorol. Soc.*, **130**, 1023-1045.

Schumann, U., 1990: Large-eddy simulation of the up-slope boundary layer. *Q. J. Roy. Meteorol. Soc.*, **116**, 637-670.

Shapiro, A., and E. Fedorovich, 2007: Katabatic flow along a differentially cooled sloping surface. *J. Fluid Mech.*, **571**, 149-175.

Shapiro A., and E. Fedorovich, 2008: Coriolis effects in homogeneous and inhomogeneous katabatic flows. *Q. J. Roy. Meteorol. Soc*., **134**, 353-370.

Shapiro A., and E. Fedorovich, 2009: Nocturnal low-level jet over a shallow slope. *Acta Geophys.*, **57**, 950-980.

Shapiro, A., B. Burkholder, and E. Fedorovich, 2012: Analytical and numerical investigation of two-dimensional katabatic flow resulting from local surface cooling. *Q. J. Roy. Meteorol. Soc*. (in press).

Sladkovic R, and H.-J. Kanter, 1977: Low-level jet in the Bavarian pre-alpine region. *Arch. Meteorol. Geoph. Bioklimatol., Ser. A*, **25**, 343-355.

Song J, K. Liao, R. L. Coulter, and B. M. Lesht, 2005: Climatology of the low-level jet at the Southern Great Plains Atmospheric Boundary Layer Experiments site. *J. Appl. Meteorol*., **44**, 1593-1606.

Stensrud, D. J., 1996: Importance of low-level jets to climate: A review. *J. Climate*, **9**, 1698-1711.

Stiperski, I., I. Kavcic, B. Grisogono, and D. R. Durran, 2007: Including Coriolis effects in the Prandtl model for katabatic flow. *Q. J. Roy. Meteorol. Soc.*, **133**, 101-106.

Whiteman, C. D., 1990: Observations of thermally developed wind systems in mountainous terrain. *Atmospheric Processes Over Complex Terrain*, W. Blumen, Ed., Amer. Meteor. Soc., 5-42.

Whiteman, C. D., X. Bian, and S. Zhong, 1997: Low-level jet climatology from enhanced rawinsonde observations at a site in the southern Great Plains. *J. Appl. Meteorol*., **36**, 1363-1376.

Zhong, S., J. D. Fast, and X. Bian, 1996: A case study of the Great Plains low-level jet using wind profiler network data and a high-resolution mesoscale model. *Mon. Weather Rev*., **124**, 785-806.

Mountain waves and Bora-like flows

Branko Grisogono
Department of Geophysics, Faculty of Science, University of Zagreb, Zagreb, Croatia

1. Introduction

Since there is no unifying theory for mesoscale dynamics, for all relevant spatio-temporal scales involved (though, there is such for synoptic-scale dynamics!), our knowledge and understanding of overall mesoscale meteorology still remains fragmented and thus, incomplete. We live in our ever changing laboratory - the atmosphere; hence, each meteorological measurement is unique and, in principle, irreplaceable. Like in the whole of geophysics, one needs and strives for: 1) high-quality measurements and field campaigns, 2) numerical (and laboratory, if possible) simulations and 3) development of succinct and robust theory.

Mountain wave theory, starting from the linear 2D and 3D wave theory, is the only systematic, consistent and self-containing theory pertaining to mesoscale meteorology. Going from linear wave theory, passing to nonlinear effects, we discuss severe down-slope windstorms, where Bora-like flows belong to (Smith 1985; 1987; Grubišić 2004; Grisogono and Belušić 2009). Namely, weak-to-moderate Bora wind can be associated with katabatic and drainage flows; however, strong and severe Bora wind, having hurricane speeds ($\approx$ 50 to 70 ms^{-1}), cannot be related to the former flows but to down-slope windstorms. Bora blows at the NE Adriatic coast as well as at a few dozens of dynamically similar places in the world. The aim of this paper and the related lecture at the Workshop is to go briefly through phases of orographic flow de-linearization, weakly-to-strongly nonlinear mountain waves, specific upslope and downslope flow responses and eventual consequences for the atmospheric boundary layer. These processes and the corresponding phenomena in the parameter space are best described briefly via vertical and horizontal Froude numbers, $Fr_v = U/(NH)$ and $Fr_h = U/(NL)$, where the former is the same as the inverse of the dimensionless mountain height, sometimes also called nonlinearity parameter (U, N, H and L are the mountain perpendicular mean wind speed, buoyancy frequency, maximum terrain height and terrain half-width along the mean wind, respectively).

2. Observations, theory and simulations

Figure 1 illustrates some of essential findings about mountain waves toward Bora-like flows, i.e., the developed strongly nonlinear mountain wave where the wave symmetry is lost.

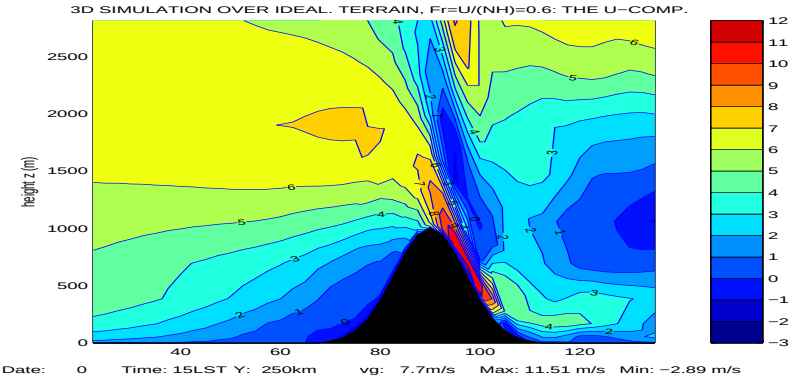

Figure 1. 3D simulation of the wind U-component, from left to right, over idealized terrain (black), for constant input parameters: vertical Froude number $Fr_v = 0.6$, the Gaussian mountain height $H = 1000$ m, half-width $L = 10$ km, half-length is 50 km (perpendicular to U). The simulation is performed with MIUU model (adopted from Grisogono and Enger 2004).

Smith (1987) and Klemp and Durran (1987) show that the experimental evidence and the corresponding numerical simulations agree that the orographic wave breaking is the main cause of this flow asymmetry represented by the low-level upstream blocking and highly distorted large-amplitude lee-side wave accompanied with a few significant phenomena. The latter include an accelerated low-level flow in the lee ($x \approx 95$ km, $z \approx 700$ m) above which there is an essentially stagnant and highly turbulent airflow ($x \approx 93$ km, $z \approx 1700$ m). Deeper in the lee there is an elevated, slow air blob due to hydraulic jump ($x \geq 120$ km, $z \sim 1000$ m) and reversed vortices (the latter two are not shown in the figure), while the area between is prone to nonhydrostatic lee waves, Kelvin-Helmholtz type of waves and the corresponding instabilities, in addition to possible boundary-layer separation and rotors.

The large-amplitude mountain wave steepens, overturns and eventually breaks due to the resonance between the incoming flow and underlying terrain so that the vertical wave length is comparable to the terrain height (usually $¼ < Fr_v \leq 1$). In this way, the mountain wave produces its own internal critical level; otherwise, the critical level may also be imposed environmentally by the incoming flow (Durran 1986; Klemp and Durran 1987; Gohm and Mayr 2005). Furthermore, the presence of a tropospheric inversion may significantly enhance the wave breaking. The secondary effects of such vigorous Bora flows can be flow pulsations (duration of several minutes) and rotors (Belušić et al. 2007; Gohm et al. 2008). Although Bora rotors were indicated more than 100 years ago in peer-review literature (see e.g., Grubišić and Orlić 2007), they have never been fully documented at the Adriatic coast. Grubišić (2004) show that in the lee of the NE Adriatic mountains there is a succession of wakes and jets, and thus potential vorticity (PV) banners, related to the mountain tops and passes.

Bora related turbulence, in particular its turbulent kinetic energy (TKE), has been studied systematically only recently (e.g., Belušić et al. 2007; Grisogono and Belušić 2009; Večenaj et al. 2010; 2012). Bora pulsations have been detected at a couple of places at the Adriatic coast having typical periods of 7 or 8 minutes; these have been simulated as well, and at least in one case these were due to Kelvin-Helmholtz instability. Still, TKE due to Bora is often misrepresented in models such as WRF (Večenaj et al. 2012). It seems that there is no unique averaging scale for deriving the Bora turbulence. For in situ measurements the averaging time scale for turbulent fluctuations should be about (15 ± 5) minutes, though it might go longer than 35 minutes; for airborne data, the averaging scale is about (1000 ± 300) m, but it might go to several km approaching a typical separation between some of more closely arranged PV banners (Večenaj 2012; Večenaj et al. 2012). Meanwhile, operational NWP models forecast three hourly mean Bora wind speeds reasonably well even up to about 2 days ahead; however, the gusts, specific locations of wind speed maxima, offshore Bora extent and detailed spatio-temporal variability are not well captured by these models yet (though, some local people know much about that). Bora rotor detection also remains an unsettled issue (typical locations, sizes, duration and movement of rotors).

3. Conclusions

Some of recent advancements in observations, modeling and theory of Bora-type flows have been presented and discussed in the light of mountain wave theory. Certain aspects of Bora related turbulence are also mentioned.

Future research should continue using more remote sensing instrumentation to analyze the onset, and cessation, details and transient phenomena during Bora wave breaking. Moreover, internal boundary layers including boundary-layer separation and rotor occurrence need to be studied (important for e.g., traffic and tourism). In terms of weak-to-moderate Bora, its interactions with katabatic or drainage flows, sea- and land-breeze should be also addressed more firmly. Furthermore, air-sea interaction including Bora episodes, which may generate the Adriatic sea convection and enhanced mixing, has to be studied more intensively prior to operational marine meteorology and coastal oceanography will provide regular and detailed local forecasts.

References

Belušić, D., M Žagar and B. Grisogono, 2007: Numerical simulation of pulsations in the bora wind. *Quart. J. Roy. Meteorol. Soc*., **133**, 1371-1388.

Durran, D.R., 1986; Another look at downslope windstorms. Part I: the development of analogs to supercritical flow in an infinitely deep, continuously stratified fluid. *J. Atmos. Sci.*, **43**, 2527-2543.

Gohm, A. and G.J. Mayr, 2005: Numerical and observational case-study of a deep Adriatic bora. *Quart. J. Roy. Meteorol. Soc*., **131**, 1363-1392.

Gohm, A., G.J. Mayr, A. Fix and A. Giez, 2008: On the onset of bora and the formation of rotors and jumps near a mountain gap. *Quart. J. Roy. Meteorol. Soc*., **134**, 21-46.

Grisogono, B. and L. Enger, 2004: Boundary-layer variations due to orographic wave-breaking in the presence of rotation. *Quart. J. Roy. Meteorol. Soc.*, **130**, 2991-3014.

Grisogono, B. and D. Belušić, 2009: A review of recent advances in understanding the meso- and micro-scale properties of the severe Bora wind. *Tellus*, **61A**, 1-16.

Grubišić, V., 2004: Bora-driven potential vorticity banners over the Adriatic. *Quart. J. Roy. Meteorol. Soc*., **130**, 2571-2603.

Grubišić, V. and M. Orlić, 2007: Early observations of rotor clouds by Andrija Mohorovičić. *Bull. Amer. Meteorol. Soc*., **88**, 693-700.

Klemp, J.B. and D.R. Durran, 1987: Numerical modelling of Bora winds. *Meteorol. Atmos. Phys.*, **36**, 215-227.

Smith, R.B., 1985: On severe downslope winds. *J. Atmos. Sci*., **42**, 2597-2603.

Smith, R.B., 1987: Aerial observations of the Yugoslavian Bora. *J. Atmos. Sci*., **44**, 269-297.

Večenaj, Ž., D. Belušić and B. Grisogono, 2010: Characteristics of the near-surface turbulence during a bora event. *Ann. Geophys*., **28**, 155-163, www.ann geophys.net/28/1/2010/.

Večenaj, Ž., 2012: Characteristics of the Bora related turbulence. *PhD dissertation*, Dept. of Geophysics, Faculty of Science, University of Zagreb, 83 pp.

Večenaj, Ž., D. Belušić, V. Grubišić and B. Grisogono, 2012: Along-coastal features of the bora related turbulence. *Bound.-Layer Meteorol*., In press, DOI: 10.1007/s10546-012-9697-6

Numerical simulation of turbulent slope flows

Evgeni Fedorovich*

**School of Meteorology, University of Oklahoma, Norman, USA*

1. Introduction

From the fluid-dynamical standpoint, the slope winds are buoyantly driven boundary-layer-type flows along heated or cooled sloping surfaces in a stratified fluid. Atmospheric researchers commonly distinguish between anabatic winds, which are driven by surface heating, and katabatic winds, which result from surface cooling (see Fig. 1).

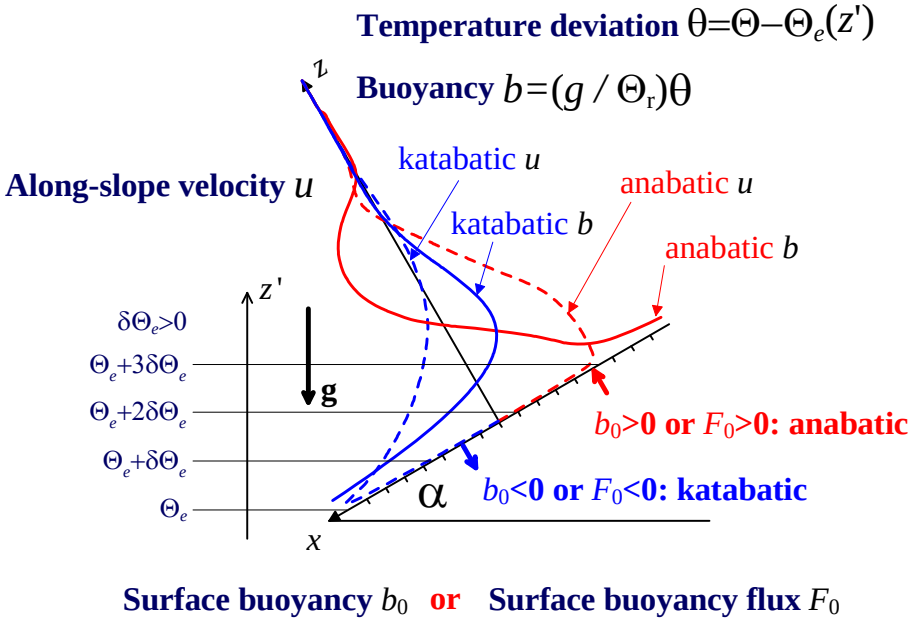

Figure 1. Schematic illustration of katabatic and anabatic flows. Surface heating/cooling may be prescribed in terms of either surface buoyancy b_0 or surface buoyancy flux F_0. The slope-following coordinates are denoted as x and z, while the vertical axis directed against the gravitational acceleration vector **g** is denoted as z'. The buoyancy b is introduced through a local potential temperature θ, environmental potential temperature Θ_e, which is a function of z' only, and constant (in lieu of commonly adopted Boussinesq approximation) reference temperature value Θ_r.

Slope flows are rather complicated fluid mechanical phenomena since they conflate three characteristic aspects of geophysical fluid dynamics: buoyant forcing, stratification, and turbulence. On larger scales, the Earth's rotation adds to this factor list, which makes formal analyses of slope winds even more complicated. There are many open questions regarding the structure of these flows and their turbulence properties. Answering these questions could be helpful for designing parameterizations of slope-wind phenomena for atmospheric models.

Prandtl (1942) proposed a first quantitative model of a slope flow that provided a conceptual view of katabatic/anabatic flows as natural-convection flows of a viscous stably-stratified fluid along a uniformly cooled or heated sloping planar surface. Prandtl's solution, which is exact within the Boussinesq framework, describes transport of environmental buoyancy toward the slope balanced by diffusion of buoyancy away from the slope, and the buoyant acceleration of the along-slope flow component balanced by the diffusion of momentum in the slope-normal direction. Later observations suggested that Prandtl's model captures principal physical mechanisms that determine the slope-flow structure. This model, in fact, is closely related to the familiar Ekman model of a homogeneous

viscous rotating fluid, which is a remarkable manifestation of the general analogy between stratified and rotating geophysical flows.

Advances in computer technology have made possible numerical modeling of turbulent slope winds and even numerical large eddy simulation (LES) of particular slope flow types. Most numerical model studies, however, reported difficulties in finding an appropriate parameterization for the near-surface portion of the flow, which is either subject to strong buoyancy damping of turbulence in the case of katabatic flow or to absolute static instability inducing convective motions above a heated surface in the case of anabatic (up-slope) wind. The LES technique (see, e.g., Schumann 1990, Skyllingstad 2003, and Axelsen and van Dop 2009), which accounts for slope-flow turbulence effects in a much more accurate and consistent manner than mesoscale models, to a certain degree overcomes this inherent shortcoming of the mesoscale modeling approach. Fundamental structural features of slope flows may also be revealed through direct numerical simulation (DNS), see, e.g., Fedorovich and Shapiro (2009). Due to the scale disparity, though, the DNS only allows exploring idealized downscaled slope-flow versions rather than real slope flows, which makes application of the DNS findings to real-world slope flows not that straightforward. Because of substantial computer resources involved and longer times needed to obtain steady flow statistics over shallow slopes, DNS runs are currently feasible only for flows along relatively steep slopes (30º and steeper).

In the lecture, recent advances in LES and DNS of turbulent non-rotating slope flows are reviewed and analyzed with an emphasis on acquiring insights into signature features of the flows important from the point of view of their modeling and parameterization.

2. Governing equations

Momentum balance equations for a small-scale (very large Rossby number) slope flow in the Boussinesq approximation are the following:

$$\frac{\partial u}{\partial t}+u\frac{\partial u}{\partial x}+v\frac{\partial u}{\partial y}+w\frac{\partial u}{\partial z}=-\frac{\partial \pi}{\partial x}+b\sin\alpha+\nu\left(\frac{\partial^2 u}{\partial x^2}+\frac{\partial^2 u}{\partial y^2}+\frac{\partial^2 u}{\partial z^2}\right), \tag{1}$$

$$\frac{\partial v}{\partial t}+u\frac{\partial v}{\partial x}+v\frac{\partial v}{\partial y}+w\frac{\partial v}{\partial z}=-\frac{\partial \pi}{\partial y}+\nu\left(\frac{\partial^2 v}{\partial x^2}+\frac{\partial^2 v}{\partial y^2}+\frac{\partial^2 v}{\partial z^2}\right), \tag{2}$$

$$\frac{\partial w}{\partial t}+u\frac{\partial w}{\partial x}+v\frac{\partial w}{\partial y}+w\frac{\partial w}{\partial z}=-\frac{\partial \pi}{\partial z}+b\cos\alpha+\nu\left(\frac{\partial^2 w}{\partial x^2}+\frac{\partial^2 w}{\partial y^2}+\frac{\partial^2 w}{\partial z^2}\right), \tag{3}$$

with the heat/buoyancy balance represented by

$$\frac{\partial b}{\partial t}+u\frac{\partial b}{\partial x}+v\frac{\partial b}{\partial y}+w\frac{\partial b}{\partial z}=-N^2(u\sin\alpha+w\cos\alpha)+\nu_h\left(\frac{\partial^2 b}{\partial x^2}+\frac{\partial^2 b}{\partial y^2}+\frac{\partial^2 b}{\partial z^2}\right). \tag{4}$$

These equations are supplemented with the continuity equation for an incompressible fluid:

$$\frac{\partial u}{\partial x}+\frac{\partial v}{\partial y}+\frac{\partial w}{\partial z}=0\,. \tag{5}$$

In the above equations, *u*, *v*, *w* are velocity components in the right-hand slope-following Cartesian coordinate system with x, y, and z being the upslope, cross-slope, and slope-normal coordinates, respectively, $\pi=[p-p_e(z')]/\rho_r$ is the normalized pressure perturbation [$p_e(z')$ is the environmental pressure, z' is the true vertical coordinate, ρ_r=const is the reference density value], $b=g[\Theta-\Theta_e(z')]/\Theta_r$ is the buoyancy, g is the gravitational acceleration, $N=\left[(g/\Theta_r)(d\Theta_e/dz')\right]^{1/2}$ is the Brunt-Väisälä (or buoyancy) frequency (where the evironmental temperature gradient $d\Theta_e/dz'$ is assumed to be constant), α is the slope angle, ν is the kinematic viscosity, and ν_h is the thermal diffusivity. The lateral boundary conditions for

prognostic variables (u, v, w, b) and normalized pressure π are periodic (so the sloping surface is supposed to be doubly-infinite along x and y). The upper boundary conditions (large z) are $\partial\varphi/\partial z = 0$, where φ is any of (u, v, w, b), and $\partial\pi/\partial z$ is obtained from (3). The surface (z=0) conditions for velocity are no-slip and impermeability (u=v=w=0), with $\partial\pi/\partial z$ obtained from (3). The surface condition for the buoyancy is either $b_{z=0} = b_0$ or $\nu_h(\partial b/\partial z)_{z=0} = -F_0$, where F_0 is the surface buoyancy flux that also has a meaning of the surface energy production rate.

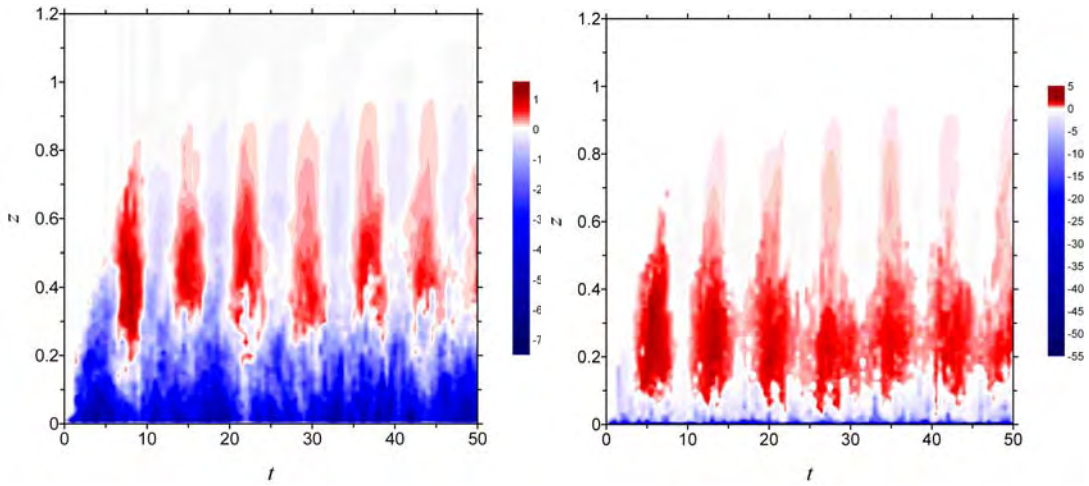

Figure 2. Temporal variations of along-slope velocity component (u, on the left, in $\mathrm{m\,s^{-1}}$) and buoyancy (b, on the right, in $\mathrm{m\,s^{-2}}$) in a katabatic flow with $F_0 = -0.5\ \mathrm{m^2 s^{-3}}$, $\nu = 10^{-4}\ \mathrm{m^2 s^{-1}}$, $N = 1\ \mathrm{s^{-1}}$ along a 60° slope at different distances from the slope in the center of the simulation domain. Distance is in meters and time is in seconds.

In DNS, the above equations are solved directly, through resolving all scales of turbulent motion from $L \sim |F_0|^{1/2} N^{-3/2}$ down to $l \sim (|F_0|^3/\nu)^{1/4}$ that is of the order of the viscous dissipation scale. The numerical algorithm employed in DNS of slope flows by Fedorovich and Shapiro (2009) directly solves (1)-(5) with assuming $\mathrm{Pr} = \nu/\nu_h = 1$. Results from that study will be reviewed and analyzed in the lecture. Spatial-temporal variations of the simulated velocity and buoyancy fields in a katabatic flow from Fedorovich and Shapiro (2009) are illustrated in Fig. 2.

3. LES of slope flows

The LES technique is based on the subdivision of the simulated turbulent fluid motions into the *resolved* motions, which are explicitly resolved on the numerical grid, and the smaller-scale *subgrid* motions whose effect is taken into account integrally through additional terms that appear in the governing equations after they are filtered using a predefined spatial filtering procedure. The concept of flow filtering used in LES is illustrated in Fig. 2. The width of the filter is related to the numerical grid spacing that is commonly assumed proportional to the characteristic length scale of subgrid turbulent motions. The filtered governing equations of the slope flow (with filtered variables indicated by tildes) appear as

$$\frac{\partial \tilde{u}_i}{\partial t} + \frac{\partial \tilde{u}_i \tilde{u}_j}{\partial x_j} = -\frac{\partial \tilde{\pi}}{\partial x_i} + \tilde{b}(\delta_{i1}\sin\alpha + \delta_{i3}\cos\alpha) + \nu\frac{\partial^2 \tilde{u}_i}{\partial x_j \partial x_j} - \frac{\partial}{\partial x_j}(\widetilde{u_i u_j} - \tilde{u}_i \tilde{u}_j), \qquad (6)$$

$$\frac{\partial \tilde{b}}{\partial t} + \frac{\partial \tilde{b}\tilde{u}_j}{\partial x_j} = -N^2(\tilde{u}_1\sin\alpha + \tilde{u}_3\cos\alpha) + \nu_h\frac{\partial^2 \tilde{b}}{\partial x_j \partial x_j} - \frac{\partial}{\partial x_j}(\widetilde{bu_j} - \tilde{b}\tilde{u}_j), \qquad \frac{\partial \tilde{u}_i}{\partial x_i} = 0, \qquad (7)$$

where i, j = 1, 2, 3; $\widetilde{u_i u_j} - \tilde{u}_i \tilde{u}_j = -\tau_{ij}^s$ is the subgrid turbulent kinematic momentum flux and $\widetilde{bu_j} - \tilde{b}\tilde{u}_j = F_j^s$ is the subgrid turbulent buoyancy flux (which is proportional to the subgrid

turbulent kinematic heat flux). In order to solve (6) and (7), one would need to prescribe closing relationships for τ_{ij}^s and F_j^s.

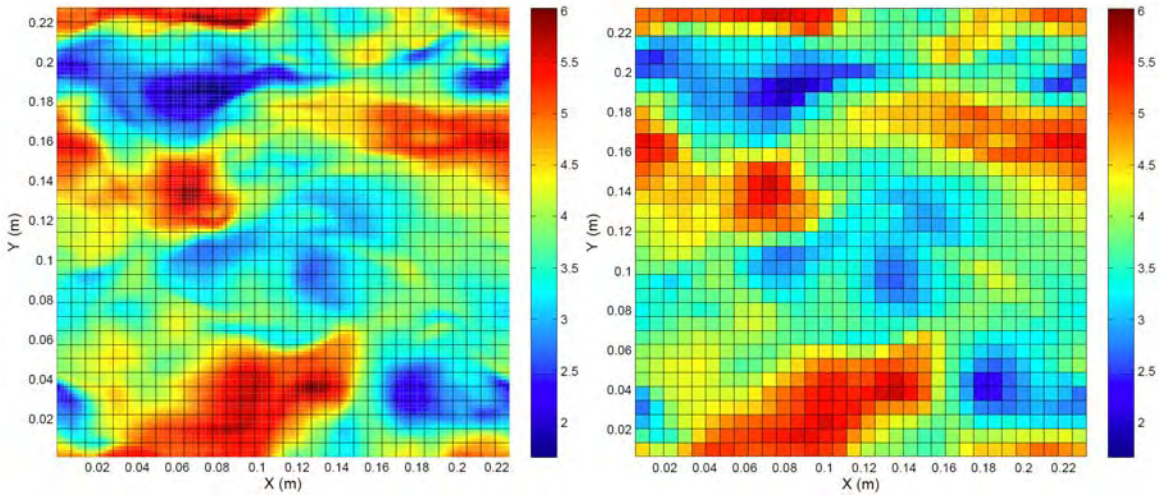

Figure 3. Illustration of application of a top-hat filter to a two-dimensional velocity field in an *X*-*Y* plane. On the left is a fine-resolved velocity field (which could be a DNS output). On the right is the filtered field that is obtained from the field on the left by filtering it to the grid four times coarser that the fine grid on the left.

Subgrid turbulence closure model that is most widely used in atmospheric LES is the model of Deardorff (1980). It is based on the prognostic equation for the subgrid turbulence kinetic energy E^s and assumes the subgrid turbulence length scale l^s proportional to the effective grid spacing (with the plugged-in reduction under conditions of strong stability). Using a Kolmogorov-Prandtl-type relationship and applying some ad-hoc assumptions, $\sqrt{E^s}$ and l^s are then combined into the subgrid turbulent diffusivities for momentum and heat, which are eventually employed to relate τ_{ij}^s and F_j^s to spatial gradients of the resolved velocity and buoyancy fields. Specifically, Deardorff's (1980) closure was employed in an extensive LES study of katabatic flows by Axelsen and van Dop (2009).

Results from that study along with examples of other LESs of slope flows will be discussed in the lecture with emphasis on the limitations of commonly employed subgrid closures when used in LES of strongly sheared and stratified slope flows (katabatic flows in particular) following findings of *a posteriori* subgrid closure evaluation study by Burkholder et al. (2010). The problem of adequate formulation of the wall functions in the LES of slope flows will also be addressed.

References

Axelsen, S. L., and H. van Dop, 2009: Large-eddy simulation of katabatic winds. Part 1: Comparison with observations. *Acta Geophysica*, **57**, 803-836.

Burkholder, B., E. Fedorovich, and A. Shapiro, 2010: Evaluating subgrid-scale models for large-eddy simulation of turbulent katabatic flow. *Quality and Reliability of Large-Eddy Simulations II*, M. V. Salvetti et al., Eds., Springer, 149-160.

Deardorff, J. W., 1980: Stratocumulus-capped mixed layers derived from a three-dimensional model. *Boundary-Layer Meteor.*, **18**, 495-527.

Fedorovich, E., and A. Shapiro, 2009: Structure of numerically simulated katabatic and anabatic flows along steep slopes. *Acta Geophysica*, **57**, 981-1010.

Prandtl, L., 1942: *Führer durch die Strömungslehre*, Vieweg und Sohn, Braunschweig, 382 pp.

Schumann, U., 1990: Large-eddy simulation of the up-slope boundary layer. *Q. J. Roy. Meteor. Soc.*, **116**, 637-670.

Skyllingstad, E. D., 2003: Large-eddy simulation of katabatic flows. *Boundary-Layer Meteor.*, **106**, 217-243.

Numerical modeling of mesoscale flows in mountainous regions [1]

Christian Barthlott

Institute for Meteorology and Climate Research (IMK-TRO)
Karlsruhe Institute of Technology (KIT), POB 3640, 76021 Karlsruhe, Germany.
E-mail: christian.barthlott@kit.edu

1. Introduction

Despite the advances in the parameterizations of physical processes and higher grid spacings of numerical weather prediction (NWP) models over the past decades, quantitative precipitation forecasting (QPF) still remains a challenge. In particular, the forecast of deep moist convection with weak synoptic forcing is still inadequate for many applications. Besides uncertain initial and boundary conditions, inaccuracies of numerical methods and/or the incomplete description of physical processes influence the performance of NWP models. For mountainous regions, several problems for QPF have been identified in recent years, e. g. an overestimation of precipitation on the windward side and a phase error in the diurnal cycle (e. g. Chaboureau *et al.*, 2004; Schwitalla *et al.*, 2008). The presence of orography is very demanding to the numerics and physics of NWP models and may also degrade forecast skill (Zängl, 2002). In addition, topographic effects on radiation become more important for mountainous areas (Buzzi, 2008).

At first, the talk will give an overview about orographic mesoscale phenomena. Then, principles and errors of numerical weather prediction will be addressed with the focus on challenges in mountainous regions. Based on three case studies, different aspects of the orographic influence on convection initiation will be presented:

1. Initiation of deep convection in the Black Forest mountains (case study from COPS: Convective and Orographically induced Precipitation Study (Kottmeier *et al.*, 2008; Wulfmeyer *et al.*, 2011))

2. Soil moisture influence on convective precipitation over complex terrain (COPS-related)

3. Relative importance of land-sea contrast and terrain height on amount and timing of convective precipitation (preliminary study for HyMeX: Hydrological cycle in the Mediterranean Experiment, http://www.hymex.org/)

2. Initiation of deep convection in the Black Forest mountains

During intensive observation period (IOP) 8b of COPS, an isolated convective cell (Fig. 1) initiated east of the Black Forest crest located in southwest Germany, although convective available potential energy was moderate only and convective inhibition was high. Measurements revealed that, due to the absence of relevant synoptic forcing, convection was initiated by local processes related to the orography. In particular, the lifting by low-level convergence in the planetary boundary layer is assumed to be the dominant process on that day. A model intercomparison with 8 representations of 5 different non-hydrostatic models was performed to identify those processes which need to be well represented to initiate convection at the right time and place. Results show, that besides an accurate specification of the thermodynamic and kinematic fields, low-level convergence lines and their ability to lift parcels up to the level of free convection need to be well represented in NWP models in order to account for their triggering effects of deep moist convection and to improve the overall forecast skill (Barthlott *et al.*, 2011).

[1] The talk will be available online at http://www.imk-tro.kit.edu/14_190.php after the workshop.

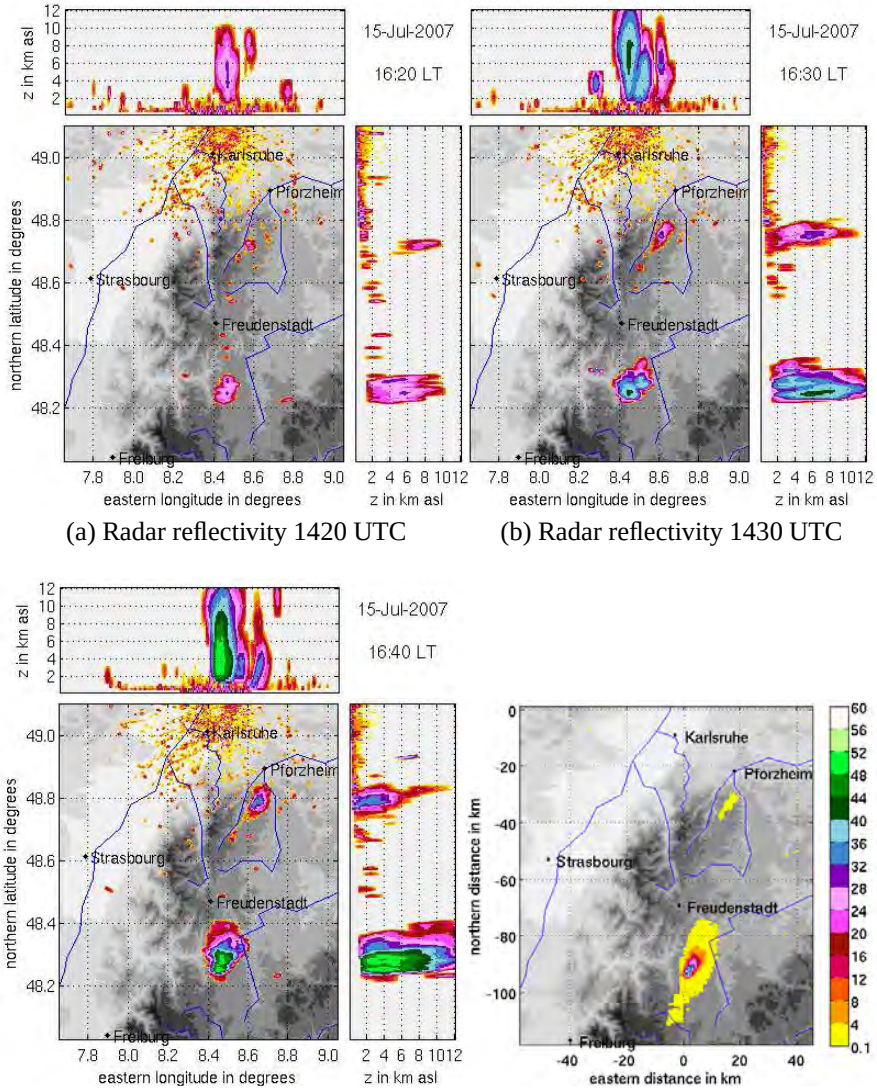

(a) Radar reflectivity 1420 UTC

(b) Radar reflectivity 1430 UTC

(c) Radar reflectivity 1440 UTC

(d) Radar-derived 24 h accumulated precipitation

Figure 1: Radar reflectivity in dBZ measured by the IMK C-band radar positioned at KIT (Campus North) from the first distinct radar echo to the mature cumulonimbus cloud (1420-1440 UTC) and derived 24 h accumulated precipitation in mm.

3. Soil moisture influence on convective precipitation over complex terrain

The influence of soil moisture on convective indices and precipitation over complex terrain is still unclear: Previous studies produced contradictory results for the existence and sign of the soil moisture-precipitation feedback, which may vary spatially and temporally. For a case study from COPS, initial soil moisture is varied from −50% to +50% of the reference run in steps of 5%. As synoptic-scale forcing is weak on the day under investigation, the triggering of convection is mainly due to soil-atmosphere interactions and boundary-layer processes. Whereas a systematic relationship to soil moisture exists for a number of variables (e. g. latent and sensible fluxes at the ground, near-surface temperature, humidity), a systematic increase of 24 h-accumulated precipitation with increasing initial soil moisture is only present in the simulations drier than the reference run (Fig. 2). That means, depending on the position of the reference soil moisture content, e. g. the further increase can lead to

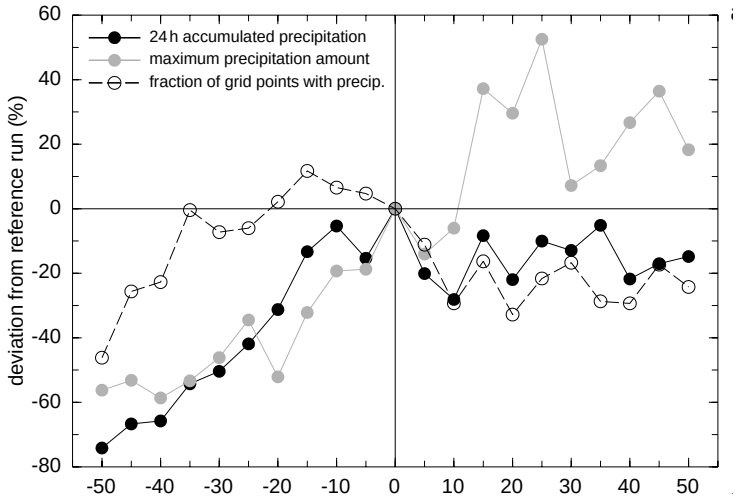

Figure 2: Deviations from the reference run as a function of different initial soil moisture contents.

both, an increased or reduced amount of precipitation (Barthlott and Kalthoff, 2011).

4. Sensitivity of deep convection to terrain forcing over Corsica

Sensitivity runs with systematically modified and removed topography (Fig. 3) are explored to evaluate the relative importance of the land-sea contrast and the terrain height for convection initiation. Whereas no convective precipitation is simulated with removed islands, all remaining simulations with flat and systematically varied terrain height show convective precipitation. In the runs with flat and reduced orography, however, convection starts around 2 h later than in the remaining runs. Therefore, an adequate representation of topographical features is important to account for the triggering effects of thermally induced wind systems. The results highlight the importance of correctly resolving the existence, strength, and inland penetration of the sea breeze and its interaction with upslope winds over mountainous islands.

References

Barthlott C, Burton R, Kirshbaum D, Hanley K, Richard E, Chaboureau JP, Trentmann J, Kern B, Bauer HS, Schwitalla T, Keil C, Seity Y, Gadian A, Blyth A, Mobbs S, Flamant C, Handwerker J. 2011. Initiation of deep convection at marginal instability in an ensemble of mesoscale models: a case-study from COPS. *Q. J. R. Meteorol. Soc.* **137 (S1)**: 118–136, doi:10.1002/qj.707.

Barthlott C, Kalthoff N. 2011. A numerical sensitivity study on the impact of soil moisture on convection-related parameters and convective precipitation over complex terrain. *J. Atmos. Sci.* **68**: 2971–2987, doi:10.1175/JAS-D-11-027.1.

Buzzi M. 2008. Challenges in operational numerical weather prediction at high resolution in complex terrain. *Swiss Federal Institute of Technology (ETH)*, doi:10.3929/ethz-a-005698833.

Chaboureau JP, Guichard F, Redelsperger JL, Lafore JL. 2004. The role of stability and moisture in the diurnal cycle of convection over land. *Q. J. R. Meteorol. Soc.* **130**: 3105–3117.

Kottmeier C, Kalthoff N, Barthlott C, Corsmeier U, Van Baelen J, Behrendt A, Behrendt R, Blyth A, Coulter R, Crewell S, Di Girolamo P, Dorninger M, Flamant C, Foken T, Hagen M, Hauck C, Höller H, Konow H, Kunz M, Mahlke H, Mobbs S, Richard E, Steinacker R, Weckwerth T, Wieser

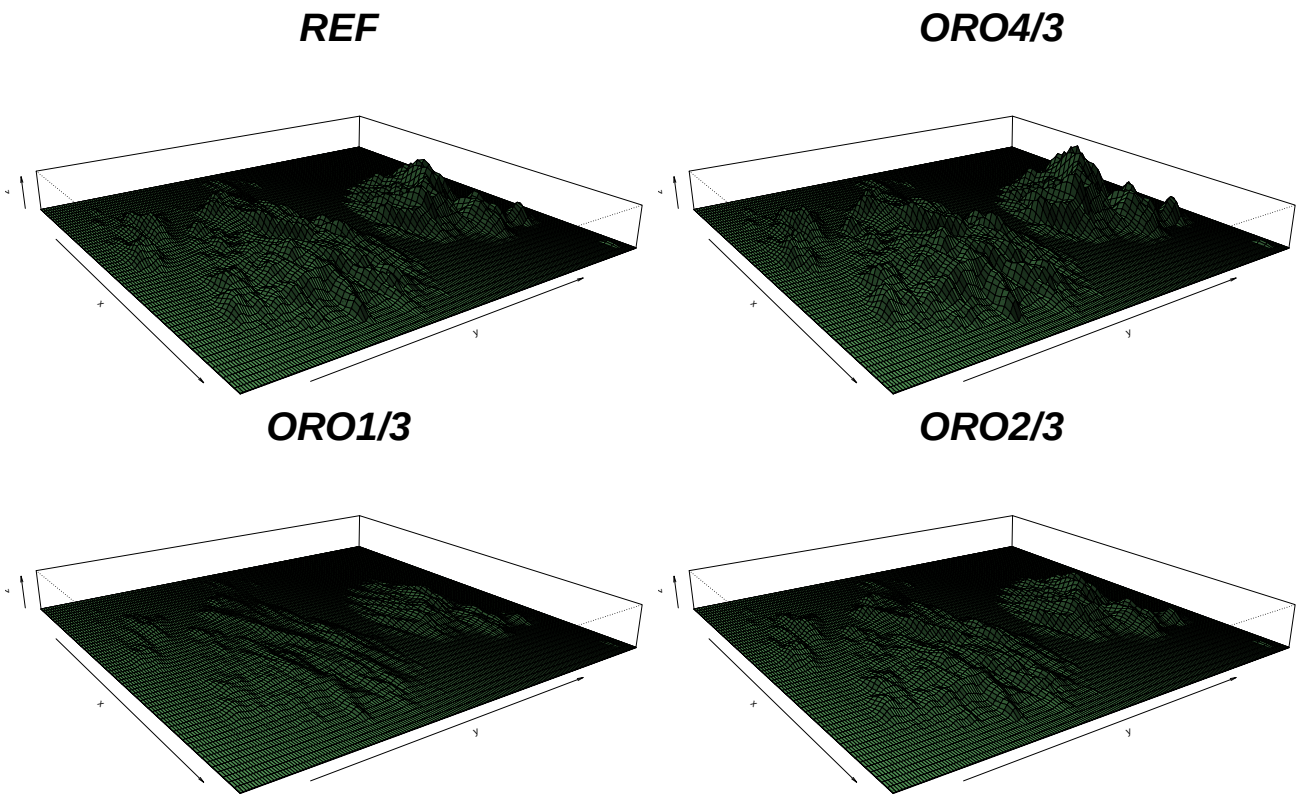

Figure 3: Modified model topography.

A, Wulfmeyer V. 2008. Mechanisms initiating deep convection over complex terrain during COPS. *Meteorol. Z.* **17**: 931–948, doi:10.1127/0941-2948/2008/0348.

Schwitalla T, Bauer HS, Wulfmeyer V, Zängl G. 2008. Systematic errors of QPF in low-mountain regions as revealed by MM5 simulations. *Meteorol. Z.* **17**: 903–919.

Wulfmeyer V, Behrendt A, Kottmeier C, Corsmeier U, Barthlott C, Craig GC, Hagen M, Althausen D, Aoshima F, Arpagaus M, Bauer HS, van Baelen J, Bennett L, Blyth A, Brandau C, Champollion C, Crewell S, Dick G, Dorninger M, Dufournet Y, Eigenmann R, Engelmann R, Flamant C, Foken T, Di Girolamo P, Groenemeijer P, Gorgas T, Grzeschik M, Peters G, Handwerker J, Hauck C, Höller H, Junkermann W, Kalthoff N, Kiemle C, König M, Krauss L, Long CN, Madonna F, Mobbs S, Neininger B, Pal S, Pigeon G, Richard E, Rotach MW, Russchenberg H, Schwitalla T, Smith V, Steinacker R, Trentmann J, Turner DD, Vogt S, Volkert H, Weckwerth T, Wernli H, Wieser A. 2011. The Convective and Orographically Induced Precipitation Study (COPS): The scientific strategy, the field phase, and first highlights. *Q. J. R. Meteorol. Soc.* **137 (S1)**: 3–30, doi:10.1002/qj.752.

Zängl G. 2002. An improved method for computing horizontal diffusion in a sigma-coordinate model and its application to simulations over mountainous topography. *Mon. Wea. Rev.* **130**: 1423–1432.

Turbulence and surface-layer parameterizations for mesoscale models

Dmitrii V. Mironov

German Weather Service, Offenbach am Main, Germany

The ensemble-mean second-order modelling framework widely used to represent (parameterize) planetary boundary-layer (PBL) turbulence in numerical models of the atmosphere, as well as of the ocean and lakes, is discussed. The discussion emphasizes parameterization assumptions that should be made in order to arrive at a reasonably simple turbulence closure. As we shall see, only a small fraction of what is currently known about the structure and transport properties of geophysical turbulence is actually used in applications such as numerical weather prediction (NWP) and climate modelling. A systematic discussion is necessary, however, in order to understand how simplified turbulence models (parameterization schemes) are obtained from rather complex second-moment equations and what is lost on the way. Importantly, a systematic consideration of the second-order modelling framework demonstrates the limits of applicability of simplified turbulence closures.

The basis for the development of second-order closure models is the set of transport equations for the second-order moments of fluctuating fields (Monin and Yaglom 1971). We first consider dry atmosphere, where the potential temperature θ is the only thermodynamic variable (θ is also referred to as simply temperature in what follows). Then, the set of governing equations consists of the equations for the Reynolds stress $\left\langle u_i' u_j' \right\rangle$, for the temperature flux $\langle u_i' \theta' \rangle$ and for the temperature variance $\langle \theta'^2 \rangle$, where u_i are the velocity components. The angle brackets denote mean quantities, and a prime denotes a deviation therefrom. Using the Boussinesq approximation and assuming that the Reynolds number is sufficiently high to neglect the molecular diffusion terms in the second-moment budget equations (a good approximation for the atmospheric flows), the second-moment equations read

$$\left(\frac{\partial}{\partial t} + \langle u_k \rangle \frac{\partial}{\partial x_k}\right) \left\langle u_i' u_j' \right\rangle = -\left(\langle u_i' u_k' \rangle \frac{\partial \langle u_j \rangle}{\partial x_k} + \left\langle u_j' u_k' \right\rangle \frac{\partial \langle u_i \rangle}{\partial x_k}\right) - \left(g_i \alpha \left\langle u_j' \theta_v' \right\rangle + g_j \alpha \langle u_i' \theta_v' \rangle\right)$$

$$-2\left(\epsilon_{imk} \Omega_m \left\langle u_k' u_j' \right\rangle + \epsilon_{jmk} \Omega_m \langle u_k' u_i' \rangle\right) + \left\langle p' \left(\frac{\partial u_i'}{\partial x_j} + \frac{\partial u_j'}{\partial x_i}\right)\right\rangle$$

$$-\frac{\partial}{\partial x_k}\left(\left\langle u_k' u_i' u_j' \right\rangle + \delta_{kj} \langle p' u_i' \rangle + \delta_{ki} \left\langle p' u_j' \right\rangle\right) - \epsilon_{ij}, \tag{1}$$

$$\left(\frac{\partial}{\partial t} + \langle u_k \rangle \frac{\partial}{\partial x_k}\right) \langle u_i' \theta' \rangle = -\langle u_k' \theta' \rangle \frac{\partial \langle u_i \rangle}{\partial x_k} - \langle u_i' u_k' \rangle \frac{\partial \langle \theta \rangle}{\partial x_k} - g_i \alpha \langle \theta' \theta_v' \rangle - 2\epsilon_{imk} \Omega_m \langle u_k' \theta' \rangle$$

$$-\left\langle \theta' \frac{\partial p'}{\partial x_i} \right\rangle - \frac{\partial}{\partial x_k} \langle u_k' u_i' \theta' \rangle - \epsilon_{\theta i}, \tag{2}$$

$$\frac{1}{2}\left(\frac{\partial}{\partial t}+\langle u_k\rangle\frac{\partial}{\partial x_k}\right)\left\langle\theta'^2\right\rangle=-\left\langle u_k'\theta'\right\rangle\frac{\partial\langle\theta\rangle}{\partial x_k}-\frac{1}{2}\frac{\partial}{\partial x_k}\left\langle u_k'\theta'^2\right\rangle-\epsilon_\theta. \tag{3}$$

Here, t is the time, x_i are the space coordinates, g_i is the acceleration due to gravity, $\alpha=-\rho^{-1}\partial\rho/\partial\theta$ is the thermal expansion coefficient, ρ is the density, Ω_i is the angular velocity of the reference frame rotation, and p is the kinematic pressure (deviation of pressure from the hydrostatically balanced pressure divided by the reference density). The Einstein summation convention for repeated indices is adopted. The last terms on the right-hand sides (r.h.s.) of the above equations are the molecular destruction (dissipation) rates of the Reynolds stress, of the temperature flux, and of the temperature variance. The quantity θ_v is the virtual potential temperature that accounts for the presence of water in the air (see below). For the case of dry air, θ_v coincides with θ. Taking the trace of Eq. (1) yields the budget equation for the turbulence kinetic energy (TKE) $\frac{1}{2}\langle u_i'^2\rangle$.

We discuss the physical meaning of various terms in the second-moment budget equations (1)–(3) and examine their role in maintaining the budgets in various flow regimes. Equations (1)–(3) are not closed as they contain a number of unknown quantities. Parameterizations (closure assumptions) are required for the dissipation rates, for the third-order velocity-velocity and velocity-temperature covariances, and for the pressure-velocity and pressure-temperature covariances to express these terms through the first-order and the second-order moments involved and thereby close the system of governing equations. A large number of parameterizations have been developed to date that vary greatly in terms of their complexity and field of application. These parameterizations are the subject of an extremely voluminous literature (see Mironov 2009 for references). We consider some parameterizations typically utilised to model geophysical flows, emphasising their advantages and limitations and their utility for modelling turbulence in the lower troposphere. Considering the third order transport terms $\left\langle u_i'u_j'u_k'\right\rangle$, $\left\langle u_i'u_j'\theta'\right\rangle$ and $\langle u_i'\theta'^2\rangle$, we compare the simplest down-gradient formulations and more complex advection-diffusion formulations (Gryanik and Hartmann 2002), where the dependence of the advection part on the skewness of velocity and temperature fields makes it possible to account for non-local transport properties of convective turbulence. We pay particular attention to the pressure scrambling terms $\left\langle p'\left(\frac{\partial u_i'}{\partial x_j}+\frac{\partial u_j'}{\partial x_i}\right)\right\rangle$ and $\left\langle\theta'\frac{\partial p'}{\partial x_i}\right\rangle$. Although the parameterization of the pressure scrambling terms is one of the key (and arguably one of the most difficult) issues in second-order turbulence modelling, it often receives unduly little attention. We examine a number of formulations, ranging from simple linear Rotta-type models (Rotta 1951, Zeman 1981) to complex strongly non-linear two-component-limit models (Craft et al. 1996, Mironov 2001). The latter models are capable of describing strongly anisotropic turbulence encountered in stable and/or rapidly rotating PBLs. Curiously, a consideration of the pressure scrambling terms is necessary to understand how the down-gradient diffusion approximation for fluxes is derived from the second-moment budget equations.

By discarding various terms in Eqs. (1)–(3) and making further simplifying assumptions, we arrive at a hierarchy of second-order closure schemes. These range from a rather complex scheme that carries non-steady transport equations for the temperature variance and for all components of the Reynolds stress and temperature flux (10 partial differential equations in the case of dry air) to highly simplified schemes where all second-moment equations are reduced to the algebraic down-gradient formulations. The so-called one-equations schemes are discussed in some detail. The only transport equation carried by those schemes is the TKE equation, whereas all other second-moment equations are re-

duced to algebraic expressions. Although one-equation TKE schemes have been and still are the draft horses of atmospheric turbulence modelling, they have many limitations and are incapable of realistically describing many flow regimes of importance in NWP, climate studies, and related applications. We discuss the added value of two-equation schemes that carry transport equations for both the TKE and the temperature variance that is characteristic of the potential energy of turbulence.

The surface-layer resistance, heat and mass transfer laws, that are used to compute surface fluxes of momentum, heat and other scalar quantities (e.g. water vapour), are discussed in some detail. We stress that the flux-profile relationships of the now classical Monin-Obukhov similarity theory (Obukhov 1946, Monin and Obukhov 1954) are consistent with the budget equations for the second-order turbulence moments. In essence, they represent the second-moment budgets truncated under the surface-layer similarity-theory assumptions, viz., (i) turbulence is continuous, stationary and horizontally-homogeneous, (ii) third-order turbulent transport is negligible, and (iii) changes of fluxes over the surface layer are small as compared to their changes over the entire PBL. Problems of the surface-layer similarity theory in conditions of vanishing mean velocity (free convection, strong static stability) are discussed.

Since the real atmosphere is moist, turbulence closure schemes should be formulated with due regard to the presence of water vapour and cloud condensate. To this end, the second-moment equations are reformulated in terms of variables that are approximately conserved for phase changes in the absence of precipitation. One pair of moist quasi-conservative variables consists of the total water specific humidity $q_t = q_v + q_l + q_i$ and the total water potential temperature $\theta_t = \theta - (\theta/T)\,(L_v/c_p)\,q_l - (\theta/T)\,(L_i/c_p)\,q_i$. Here, q_v is the specific humidity, q_l is the liquid water specific humidity, q_i is the solid water specific humidity (the mass of cloud ice per unit mass of moist air), c_p is the specific heat of air at constant pressure, L_v is the specific heat of vapourisation, L_i is the specific heat of sublimation, and T is the absolute temperature. For moist atmosphere, Eqs. (1)–(3) remain the same to within the substitution of θ_t for θ, and additional equations for the flux $\langle u_i' q_t' \rangle$ and the variance $\langle q_t'^2 \rangle$ of the total water specific humidity and for the temperature-humidity covariance $\langle \theta_t' q_t' \rangle$ should be used. The virtual potential temperature θ_v that enters the buoyancy terms in the Reynolds-stress and scalar-flux equations is introduced with due regard for the water loading effect, $\theta_v = \theta\,[1 + (R-1)\,q_v - q_l - q_i]$, where $R = R_v/R_d$ is the ratio of the gas constants for water vapour and for dry air. Some tricky issues related to modelling moist atmospheric turbulence are briefly discussed, e.g. the effect of clouds on the buoyancy production/destruction of the Reynolds stress and scalar fluxes, and the representation of the fractional cloud cover (Tompkins 2005).

We give an example of how large-eddy simulations (LES) can be used to get insight into the structure and transport properties of turbulence and to improve turbulence models. Using a data set generated by LES, Mironov and Sullivan (2010) performed a detailed comparative analysis of the second-moment budgets in the stably stratified PBLs over temperature-homogeneous and temperature-heterogeneous surfaces. The budget of temperature variance proved to be the key to understanding enhanced mixing in the heterogeneous PBL, Fig. 1. The analysis revealed an important role of the third-order transport term in the temperature-variance budget that is often neglected in the turbulence models of the stably stratified PBL.

Finally, some challenging issues in second-order turbulence modelling of geophysical flows are outlined.

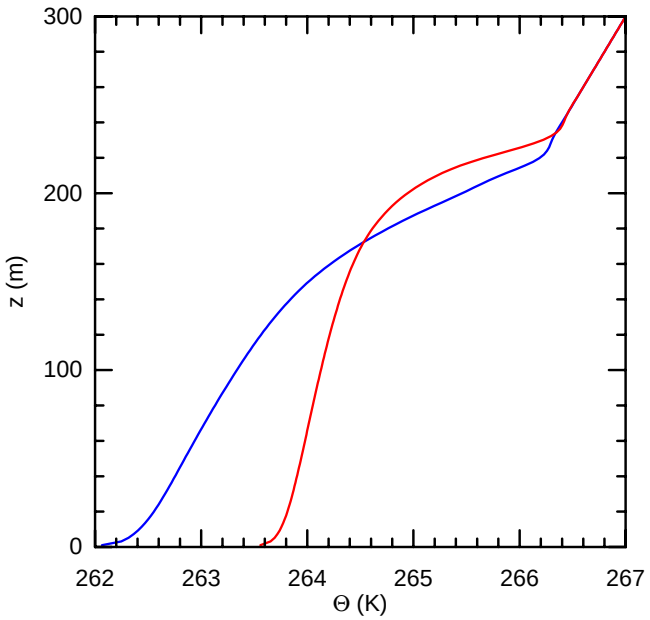

Figure 1: Mean potential temperature from LES of the stably stratified PBLs over homogeneous (blue) and heterogeneous (red) surfaces. The PBL over temperature-heterogeneous surface is deeper and is better mixed as compared to its homogeneous counterpart.

References

Craft, T. J., N. Z. Ince, and B. E. Launder, 1996: Recent developments in second-moment closure for buoyancy-affected flows. *Dyn. Atmos. Oceans*, **23**, 99–114.

Gryanik, V. M., and J. Hartmann, 2002: A turbulence closure for the convective boundary layer based on a two-scale mass-flux approach. *J. Atmos. Sci.*, **59**, 2729–2744.

Mironov, D. V., 2001: Pressure-potential-temperature covariance in convection with rotation. *Quart. J. Roy. Meteorol. Soc.*, **127**, 89–100.

Mironov, D. V., 2009: Turbulence in the lower troposphere: second-order closure and mass-flux modelling frameworks. *Interdisciplinary Aspects of Turbulence*, Lect. Notes Phys., **756**, W. Hillebrandt and F. Kupka, Eds., Springer-Verlag, Berlin, Heidelberg, 161–221. doi: 10.1007/978-3-540-78961-1 5

Mironov, D. V., and P. P. Sullivan, 2010: Effect of horizontal surface temperature heterogeneity on turbulent mixing in the stably stratified atmospheric boundary layer. *Proc. 19th Amer. Meteorol. Soc. Symp. on Boundary Layers and Turbulence*, Keystone, CO, USA, paper 6.3, 10 pp.

Monin, A. S., and A. M. Obukhov, 1954: Basic laws of turbulent mixing in the atmospheric surface layer. *Trudy Geofiz. Inst. Akad. Nauk SSSR*, No. 24 (151), 163–187.

Monin, A. S., and A. M. Yaglom, 1971: *Statistical Fluid Mechanics*. Vol. 1. MIT Press, Cambridge, Massachusetts, 769 pp.

Obukhov, A. M., 1946: Turbulence in an atmosphere with a non-uniform temperature. *Trudy Inst. Teor. Geofiz. Akad. Nauk SSSR*, **1**, 95–115. (English translation: *Boundary-Layer Meteorol.*, 1971, **2**, 7–29.)

Rotta, J. C., 1951: Statistische Theorie nichthomogener Turbulenz. 1. *Zs. Phys.*, **129**, 547–572.

Tompkins, A. M., 2002: A prognostic parameterization for the subgrid-scale variability of water vapor and clouds in large-scale models and its use to diagnose cloud cover. *J. Atmos. Sci.*, **59**, 1917–1942.

Zeman, O., 1981: Progress in the modelling of planetary boundary layers. *Ann. Rev. Fluid Mech.*, **13**, 253–272.

Observational Studies of Mesoscale Flows in Complex Topography

C. David Whiteman

Atmospheric Sciences Department, University of Utah, Salt Lake City, UT USA

1. Introduction

In connection with this talk, we plan to hand out a recent book chapter by Zardi and Whiteman (2012) that is a comprehensive and up-to-date review of diurnal mountain wind systems, including many references. Thus, the in-workshop presentation will survey only the main highlights of this topic and will focus on newly completed research, illustrating the great variety of interesting mesoscale flows. Included is information on the diurnal mountain wind systems that affect entire mountain ranges, valleys, and slopes, as well as the meteorology of basins. New results from observational studies in basins will be featured, including newly discovered cold and warm air intrusions into basins, the formation of cross-basin winds and hydraulic flows, and the air quality implications of persistent cold-air pools in urban mountain basins. While most of the examples come from research during clear, undisturbed conditions, the talk will be concluded with an example of moist mesoscale flows that produce spectacular deposits of rime ice on isolated peaks in Patagonia (Figure 1).

2. Outline of Oral Presentation

Introduction to Diurnal Mountain Winds
- Terminology
- Inhomogeneous and non-stationary flows in mountains

Mountain-Plain Wind System
- Overview
- The horizontal pressure gradients that drive them
- Example from U.S. high plains
- Example from the Alps

Slope Wind System
- Up- and down-slope flows
- Video of downslope flow in an Alpine basin

Valley Wind System
- How does their presence affect wind climatologies?
- Their physical mechanisms and the topographic amplification factor
- The run-out of down-valley winds onto a plain
- Valley exit jets
- Aberrant valley winds
  - Winds at the Maloja Pass
  - Winds at a turn in the Rivieratal
  - The Ora del Garda wind
  - Wind channeling

Cross-valley winds

Diurnal Cycle of Mountain Winds

Basin Meteorology
- Why do we get such cold temperature minima in basins?
- Meteorological factors that break up basin inversions
- Things we have learned from the Meteor Crater experiments
  - Cold air intrusions

Hydraulic flows
Cross-basin winds
Persistent wintertime cold-air pools
Temperature structure in a deep open-pit copper mine
Rime mushrooms on mountains: Their causes and impacts on mountaineering
Summary

References

Zardi, D., and C. D. Whiteman, 2012: Diurnal Mountain Wind Systems. Chapter 2 in: *Mountain Weather Research and Forecasting* (Chow, F. K., S. F. J. DeWekker, and B. Snyder (Eds.)). Springer, Berlin. In press.

Contact information:
Prof. Dave Whiteman
Atmospheric Sciences Department
University of Utah
135 S 1460 E, Rm 819
Salt Lake City, UT 84112-0110 USA
dave.whiteman@utah.edu

Figure 1. A sequence of rime mushrooms covers the southwest ridge of Cerro Paine Grande in Argentine Patagonia. How do these mushrooms form? How does the meteorology and climate affect their formation? What effects do the rime mushrooms have on mountaineering? © Rolando Garibotti

Interactions Between Mesoscale Convection and the Environment

David J. Raymond*

*Dept. of Physics and Geophysical Research Center, New Mexico Tech, Socorro, NM, USA

A great deal of work has gone into understanding the detailed structure and dynamics of mesoscale convective systems. In this presentation I take a somewhat different approach which has arisen out of the study of deep convection over tropical oceans. Rather than being concerned with morphological details, the overall dynamic and thermodynamic interaction of mesoscale convective systems with the surrounding environment is examined. This interaction consists of two parts, the effect of the environment on the convection and the effect of the convection on the environment. The thermodynamic interactions with the environment are discussed first, followed by the dynamic interactions mediated by the potential vorticity.

Effect of environment on convection

The weak temperature gradient approximation (WTG; Sobel et al. 2001) began as a dynamical model for large-scale motion in the tropics. In essence, gravity waves are assumed to redistribute buoyancy perturbations with high efficiency in the tropics, resulting in weak horizontal and temporal gradients of virtual temperature there. This idea has also been applied to the problem of lateral boundary conditions for cloud-resolving model calculations (CRMs; Raymond and Zeng 2005). In this application, the mean virtual temperature profile in the model is relaxed to a reference profile representative of the environment surrounding the convection. The cooling required to produce this balance is equal to the net heating profile in the CRM due convection and radiation. The vertical motion that would have induced this cooling via dry adiabatic lifting is called the WTG vertical velocity. The moisture advective tendency produced by the WTG vertical velocity is also incorporated into the CRM, as well as entrainment of air from lateral inflows demanded by mass continuity with the vertical motion. Though the large-scale aspects of WTG are specific to the tropics, the related CRM lateral boundary conditions apply at higher latitudes as long as the horizontal dimensions of the CRM are smaller than the Rossby radius. The WTG vertical velocity times the air density is interpreted as the mean vertical mass flux profile produced by the convection.

Recent work using a CRM in WTG mode (Raymond and Sessions 2007) has shown that mean vertical mass flux profiles of mesoscale convective systems over tropical oceans are strong functions of environmental temperature and moisture profiles. In particular, top-heavy mass flux profiles are associated with strong convective instability and a dry mid-troposphere, whereas bottom-heavy profiles occur in moist, stable environments. Top-heavy profiles are generally symptomatic of intense but isolated mesoscale convective systems, while the bottom-heavy case is characteristic of weaker convection producing widespread rainfall. The latter typically results in more precipitation on the average than the former.

Effect of convection on the environment

Mesoscale convective systems influence the surrounding thermodynamic environment in two ways: (1) they extract moisture from the atmosphere in the form of rainfall; (2) they redistribute the moist entropy (hereafter known simply as "entropy"). The entropy is approximately conserved by moist adiabatic processes and is a useful proxy for moisture, as temperature profiles often change little with time.

The thermodynamic effect of convection on the atmosphere is summarized in the concept of normalized gross moist stability (NGMS; Neelin and Held 1987, Raymond et al. 2009). This quantity is the ratio of the vertical integrals of the horizontal divergence of entropy and the

horizontal convergence of moisture. Multiplication of the entropy divergence by a constant reference temperature and the moisture convergence by the latent heat of condensation serves to non-dimensionalize this quantity. Large values of the NGMS result in strong drying of the environment, which inhibits the subsequent development of convection. Bottom-heavy mass flux profiles and higher values of mid-level humidity yield smaller values of the NGMS, which favors the subsequent development of convection.

Convection and potential vorticity

Though convection can change nearby environmental temperatures, these temperature fluctuations relax rapidly (typically less than 1 day) to a state of thermal wind balance as gravity waves carry off unbalanced buoyancy anomalies. This "relax to balance" behavior is a mid-latitude extension of the tropical weak temperature gradient condition. Relax to balance does not occur as readily in the planetary boundary layer, where the rigid lower boundary and surface friction play complicating roles.

The natural way to determine the balanced state of the atmosphere outside the boundary layer is to invert the potential vorticity distribution subject to the appropriate balance condition (Hoskins et al. 1985). Geostrophic balance is often a good approximation, though for more intense systems it may be necessary to use nonlinear balance (Davis 1992, Raymond 1992). Thus, the manner in which convection can alter the temperature structure of the atmosphere (outside of the boundary layer) is via its effect on the potential vorticity.

Convection rearranges the potential vorticity distribution of the free troposphere according to a well-developed theory (Haynes and McIntyre 1987). One frequent consequence is the creation of mid-level mesovortices. Top-heavy convection with its strong mid-level inflow concentrating vorticity is responsible for this mid-level spinup. The resulting balanced temperature response is a cool anomaly below the mesocyclone and a warm anomaly above. This increases the buoyancy of parcels below the vortex and decreases it above, resulting in more bottom-heavy convection. Such convection turns out to exhibit lower values of the NGMS, which means less drying occurs in the environment, making it more favorable for the development of subsequent convection (Raymond et al. 2011). This mechanism is likely to be important for tropical cyclogenesis and it may help explain why pre-existing mesoscale convective vortices in middle latitudes are favored locations for convective re-development.

References

Davis, C. A., 1992: Piecewise potential vorticity inversion. *J. Atmos. Sci.,* **49,** 1397-1411.

Haynes, P. H., and M. E. McIntyre, 1987: On the evolution of vorticity and potential vorticity in the presence of diabatic heating and frictional or other forces. *J. Atmos. Sci.*, **44**, 828-841.

Hoskins, B. J., M. E. McIntyre, and A. W. Robertson, 1985: On the use and significance of isentropic potential vorticity maps. *Quart. J. Roy. Meteor. Soc.,* **111,** 877-946.

Neelin, J. D., and I. M. Held, 1987: Modeling tropical convergence based on the moist static energy budget. *Mon. Wea. Rev.,* **115,** 3-12.

Raymond, D. J., 1992: Nonlinear balance and potential-vorticity thinking at large Rossby number. *Quart. J. Roy. Meteor. Soc.,* **118,** 987-1015.

Raymond, D. J. and S. L. Sessions, 2007: Evolution of convection during tropical cyclogenesis. *Geophys. Res. Letters,* **34,** L06811, doi:10.1029/2006GL028607.

Raymond, D. J., S. L. Sessions, and C. López Carrillo, 2011: Thermodynamics of tropical cyclogenesis in the northwest Pacific. *J. Geophys. Res.,* **116,** D18101, doi:10.1029/2011JD015624.

Raymond, D. J., S. Sessions, A. Sobel, and Ž. Fuchs, 2009: The mechanics of gross moist stability. *J. Adv. Model. Earth Syst.*, **1**, art. #9, 20 pp.

Raymond, D. J., and X. Zeng, 2005: Modelling tropical atmospheric convection in the context of the weak temperature gradient approximation. *Quart. J. Roy. Meteor. Soc.*, **131**, 1301-1320.

Sobel, A. H., J. Nilsson, and L. M. Polvani, 2001: The weak temperature gradient approximation and balanced tropical moisture waves. *J. Atmos. Sci.*, **58**, 3650-3665.

Data assimilation in mesoscale modeling and numerical weather prediction

Nils Gustafsson*

**Swedish Meteorological and Hydrological Institute, Norrköping, Sweden*

In comparison with data assimilation for synoptic scales, which is well established since many years, data assimilation for mesoscale modeling and numerical weather prediction is in its infancy. One important reason is the lack of the knowledge on adequate balance relations for the mesoscale, similar to the geostrophic balance relationship for synoptic scales. A related reason is the increased importance of non-linear processes and, in particular, non-linear moist processes. Non-linearities will give rise to flow-dependencies that need to be handled (and utilized) in the mesoscale assimilation process. Non-linearities also have the effect to reduce the predictability for model variables affected by, for example, moist physical processes. Furthermore, establishment of non-Gaussian forecast error probability distributions that are difficult to handle with traditional data assimilation techniques is another effect of non-linear processes.

The intention is to describe and discuss the following aspects of mesoscale data assimilation during the workshop presentation:

(1) The relative importance of different model variables in the initial conditions for mesoscale models;
(2) An overview of assimilation techniques for the mesoscale including variational techniques, ensemble techniques and nudging;
(3) Particular problems in the assimilation of moisture variables;
(4) Assimilation of radar and satellite information for the mesoscale prediction.

Satellite data in subsynoptic-scale meteorology

Nataša Strelec Mahović

Meteorological and Hydrological Service, Zagreb, Croatia

1. Introduction

In the analysis and nowcast of subsynoptic-scale weather features satellite data, together with other remote sensing data such as radar and lightning data, play an extremely important role. The reason lies in the fact that the operational NWP models are usually not completely capable of resolving the features on subsynoptic scale with all their characteristics.

In this lecture the focus will be on the use of Meteosat SEVIRI (Spinning Enhanced Visible and Infra-Red Imager) data in the analysis and nowcast of subsynoptic-scale weather phenomena. Most weight will be given to the analysis of convective development, since it usually attracts most attention in the forecasters community.

Satellite data have proven to be a useful tool in the analysis of all phases of convective development, therefore it will be shown how different types of satellite data and products can be applied in different development phases. Additionaly, some other mesoscale phenomena seen in the satellite data will be shown.

2. Pre-convective environment

The term applies to to the 4-D thermodynamic and wind field present before the initiation of convection. Multispectral satellite data, combined with temperature and moisture profiles from a NWP model, provide an estimate of convective instability and moisture availability in near-real time (15 or 5 min slots) with rather high spatial resolution. This is a big advantage over 12-hour resolution and often coarsely spaced radiosonde profiles.

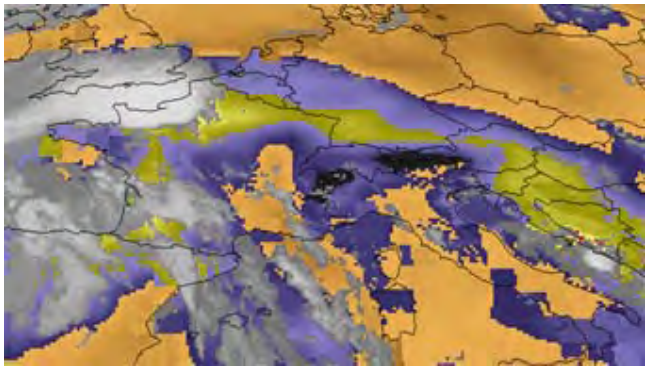

Figure 1. K index obtained by physical retrieval from Meteosat 9 data

Besides such stability parameters, a combination of WV imagery and satellite-derived winds (Bedka and Mecikalski, 2005) as well as NWP model winds is used to identify jet stream, vorticity maxima and tropospheric potential vorticity anomalies defining the regions where synoptic-scale forcing mechanisms are favourable for convective storm development. A forecaster can use these methods to estimate locations of future convective development and potential storm severity with a 6+ hour lead-time.

3. Convective Initiation (CI)

The term "convective initiation" refers to the process where an existing cumulus cloud begins rapid vertical growth. During the CI process, a convective cloud top cools and eventually glaciates. Different methods have been developed to objectively identify convective clouds and cloud-top temperature changes and make nowcasts using time sequences of multispectral imagery. Depending on the data source used to define CI and the vigor of convective development, existing methods have been shown to offer up to a 90-minute nowcast lead-time.

Table 1: MSG satellite related IR interest field use in the CI algorithm. From Mecikalski (2007).

MSG CI Interest Field	Critical Value	Physical Interpretation & Comments
[1] 10.8 μm T_B [*IF1*]	< 0° C	Cloud-top coldness
[2] 10.8 μm T_B Time Trend [*IF2, IF3*]	< –4° C/15 mins ΔT_B/30 min < ΔT_B/15 min	Cloud growth rates
[1] 10.8 μm T_B drop to <0° C [*IF4*]	Within prior 30 mins	Cloud-top glaciation
[1] 6.2 – 10.8 μm difference [*IF5*]	–30° C to –10° C	Cloud growth into dry air aloft
[1] 6.2 – 10.8 μm Time Trend [*IF6*]	> 2-3° C/15 mins	Cloud growth rates into dry air aloft
[2] 13.4 – 10.8 μm difference [*IF7*] 12.0 – 10.8 μm difference	–25° C to –5° C 0 to –3° C	Cloud growth information, into mid- and upper troposphere (redundant)
[2] 13.4 – 10.8 μm Trend [*IF8*] 12.0 – 10.8 μm Trend	> 3° C/15 mins > 1° C/15 mins	Cloud growth rate information, into mid- and upper- troposphere (redundant)
[1] 3.8 – 10.8 μm difference [*IF9*]	Transition across 0° C in 15-30 min	Cloud-top glaciation (see also Rosenfeld et al. 2008)
[1] 3.8 – 10.8 μm Time Trend [*IF10*]	> |-5| ° C	Cloud-top glaciation (see also Rosenfeld et al. 2008)
[1] 7.3 – 10.8 μm difference [*IF11*]	–40° C to –15° C	Cloud growth into dry air aloft (may be redundant with 6.2–10.8 μm)
[1] 7.3 – 10.8 μm Time Trend [*IF12*]	> 3-4° C/15 mins	Cloud growth rates into dry air aloft (may be redundant with 6.2–10.8 μm)
[1] 1.6 – 10.8 μm difference [*IF13*]	Look-up table for microphysics and glaciation (0-1)	Cloud-top glaciation (daytime only)
[1] 1.6 – 10.8 μm Time Trend [*IF14*]	Positive trend towards +1	Cloud-top glaciation rates (daytime only)
[1] 8.7 – 10.8 μm difference [*IF15*] 8.7 – 12.0 μm difference	Look-up table for microphysics; < 0° C (use existing product)	Cloud-top glaciation towards precipitation formation
[1] 8.7 – 10.8 μm Time Trend [*IF16*]	-2-5° C/15 min	Cloud-top glaciation rates towards precipitation formation
[1] 6.2 – 7.3 μm difference [*IF17*]	Positive difference	Assessing if cumulus broke capping inversion
[19] CI Indicators		

4. Mature convection

The term "mature convective storm" discribes an individual or organized cluster of convective clouds with tops at or above their local equilibrium level. They can range in size and organization from a single air-mass thunderstorm to a mesoscale convective system. Mature convective storms are the regions of strong vertical motions (updrafts) that advect ice hydrometeors into the upper troposphere and lower stratosphere.

In this phase of convective development multispectral satellite brightness temperatures and brightness temperature differences are used to identify locations of hazardous deep convective storms and the regions within them that may be severe. Spatial brightness temperature patterns, near-

IR ice particle size retrievals (Rosenfeld et al., 2008), and RGB composites are used to identify features such as above anvil cirrus plumes, overshooting convective cloud tops (Bedka, 2011; Mikuš and Strelec Mahović, 2011), cold- U/V and cold ring signatures (Setvak et al., 2010) etc.

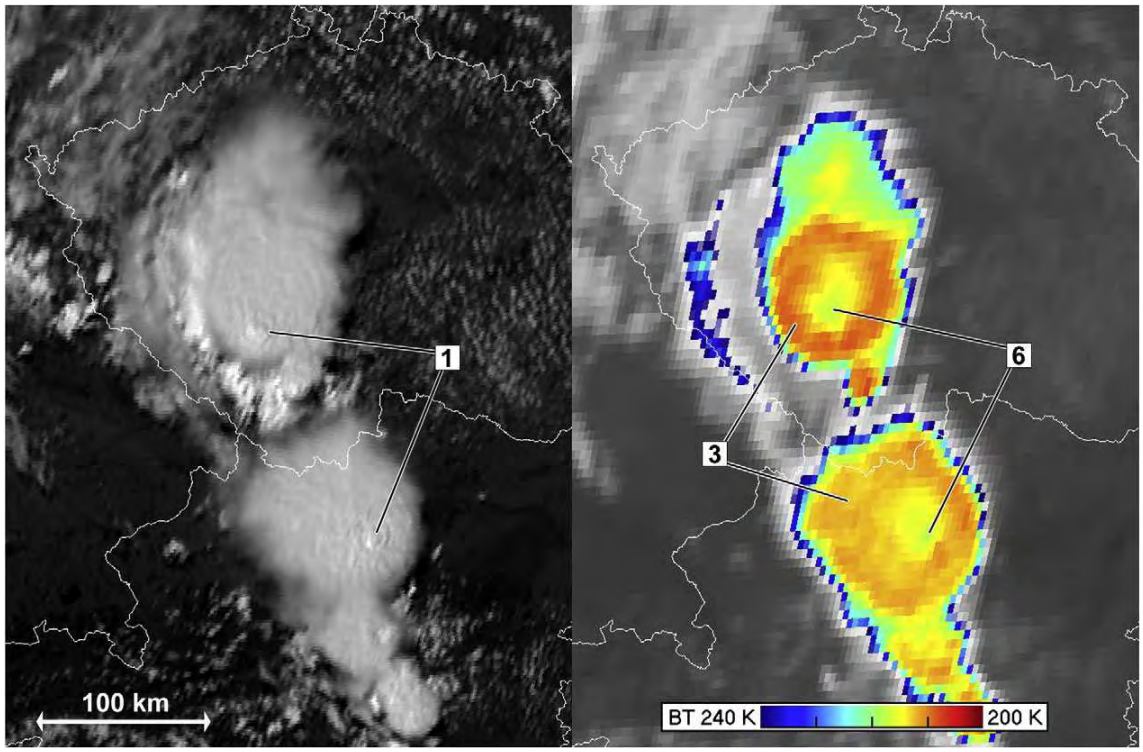

Figure 2. Examples of cold-ring shaped storms (Meteosat-8, 25 June 2006,13:45 UTC, Czech Republic and Austria). Left: high-resolution visible (HRV) image, right: color enhanced IR10.8 image. Legend: 1–overshooting tops, 3–cold ring shapes, 6–central warmspots (CWS) (Setvak, 2010).

5. Other mesoscale weather features revealed by the satellite images

Besides convective clouds there is a whole palette of the subsynoptic-scale weather features which can be recognized in the satellite data, especially in the high-resolution visible (HRV) images and in the RGB combinations of images.

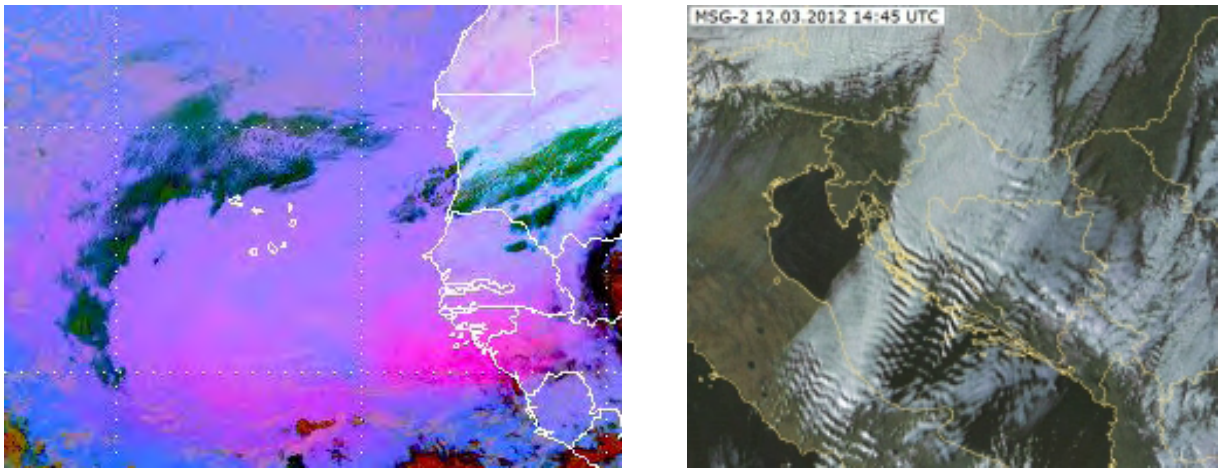

Figure 3. Dust RGB showing dust cloud leaving African coast (left) and lee waves as seen in the Meteosat HRV image (right).

Some of them will be shown and discussed, such as dust storms, topographically induced cloud features, fog/low clouds etc.

References

Bedka, K. M. and J. R. Mecikalski, 2005: Application of Satellite-Derived Atmospheric Motion Vectors for Estimating Mesoscale Flows. *J. Appl. Meteor*., **44**, 1761–1772.

Bedka, K. M., 2011: Overshooting cloud top detections using MSG SEVIRI infrared brightness temperatures and their relationship to severe weather over Europe. *Atmos.Res.*, **99**, 175-189.

Berendes T. A., J. R. Mecikalski, W. M. MacKenzie Jr., K. M. Bedka, and U. S. Nair, 2008: Convective cloud identification and classification in daytime satellite imagery using standard deviation limited adaptive clustering. *J. Geophys. Res*., **113**, D20207, doi:10.1029/2008JD010287.

EUMETSAT Convection Working Group Best Practice document: http://www.convection-wg.org/doc_meci/best_practise_CWG_v3.pdf

Mecikalski, J.R., 2007: Satellite-based Convective Initiation Nowcasting System Improvements Expected from the MTG FCI Meteosat Third Generation Capability, EUM/CO/07/4600000405/JKG Technical Report, http://www.eumetsat.int/groups/pps/documents/document/pdf_mtg_rep35.pdf

Mikuš, P. and N. Strelec Mahović, 2011: Correlating overshooting tops and severe weather. 6th European Conference on Severe Storms (ECSS 2011), 3-7 October 2011, Palma de Mallorca, Balearic Islands, Spain.

Rosenfeld, D., W. L. Woodley, A. Lerner, G. Kelman, and D. T. Lindsey, 2008: Satellite detection of severe convective storms by their retrieved vertical profiles of cloud particle effective radius and thermodynamic phase. *J. Geophys. Res.*, **113**, D04208, doi:10.1029/2007JD008600.

Setvak, M., D. T. Lindsey, P. Novak, P. K. Wang, M. Radova, J. Kerkmann, L. Grasso, S. Su, R. M. Rabin, J. Stastka, and Z. Charvat, 2010: Satellite-observed cold-ring-shaped features atop deep convective clouds. *Atmos. Research*, **97**, 80-96.